01 May 2004

A Sequential Approach to Modeling Catalytic Reactions in Packed-Bed Reactors

Jing Guo

Muthanna H. Al-Dahhan
Missouri University of Science and Technology, aldahhanm@mst.edu

Recommended Citation

J. Guo and M. H. Al-Dahhan, "A Sequential Approach to Modeling Catalytic Reactions in Packed-Bed Reactors," *Chemical Engineering Science*, vol. 59, no. 10, pp. 2023 - 2037, Elsevier, May 2004.
The definitive version is available at https://doi.org/10.1016/j.ces.2004.01.048

ELSEVIER

Chemical Engineering Science 59 (2004) 2023–2037

Chemical Engineering Science

www.elsevier.com/locate/ces

A sequential approach to modeling catalytic reactions in packed-bed reactors

Jing Guo, Muthanna Al-Dahhan*

Department of Chemical Engineering, Chemical Reaction Engineering Laboratory (CREL), Campus Box 1198, Washington University, St. Louis, MO 63130, USA

Received 28 April 2003; received in revised form 11 November 2003; accepted 15 January 2004

Abstract

A sequential modeling approach is proposed to simulate catalytic reactions in packed-bed reactors. The hydrogenation of alpha-methylstyrene and wet oxidation of phenol are selected as studied cases. The modeling scheme combines a reactor scale axial dispersion model with a pellet scale model. Without involving any fitting parameters, such an approach accounts for the non-linear reaction kinetics expression and different types of pellet–liquid wetting contact. To validate the developed modeling scheme and the parallel approach reported in the literature, the experimental observations for hydrogenation of alpha-methylstyrene to cumene have been employed. The predicted results by both approaches agree reasonably with the experimental data for both gas- and liquid-limited reaction. The proposed sequential approach was also used to simulate the dynamic performance of the reactor and pellets for the catalytic wet oxidation of aqueous phenol over a newly developed but rapidly deactivated catalyst (MnO_2/CeO_2). The simulation results for the catalytic wet oxidation process by both approaches were compared. The simulation describes the time evolution of the catalyst stability at different pellet points along the reactor axis. The performance of trickle beds and packed bubble columns over a range of operating conditions were also investigated, and packed bubble columns were found to achieve higher phenol conversion at the cost of more rapid catalyst deactivation.

Keywords: Catalysis; Catalyst deactivation; Chemical reactors; Axial dispersion model; Multiphase reactions; Packed bed

1. Introduction

Trickle-bed reactors (TBRs) or packed-bed bubble columns (PBC) are multiphase catalytic reactors with cocurrent two-phase downflow or upflow used for processing gaseous and liquid reactants over solid catalysts. They are widely used in the chemical, petrochemical, and petroleum industries, for tasks such as oxidation of sulfur dioxide to sulfur trioxide (Goto and Smith, 1975) and hydrogenation of vegetable oils (Ramachandran and Chaudhari, 1983). New commercial and potential applications of packed-bed reactors include waste stream treatment, which is now applied to the oxidation of organic compounds in industrial aqueous effluents. Such an application is especially useful to replace biofilters when a high organic concentration inhibits bacteria development (Yurii and Moshe, 1998).

Due to gas and liquid flowing concurrently through the catalyst-bed, packed-bed performance depends on a complex interaction of the intraparticle and interphase mass transport, reaction kinetics, and hydrodynamics. Many reports on experimental and modeling work involving packed-bed reactors have been published with the aim of comparing the predictions with experimental data and understanding the interplay between overall reactor performance and various factors affecting it (Goto and Smith, 1975). Among the reactor scale model, the plug-flow model has been used for modeling a large TBR (Froment et al., 1994). To account for the maldistribution and non-uniformity of two-phase flow, several other reactor scale models have been proposed in the literature. The axial dispersion model (ADM) is the simplest model describing differential mixing in packed-bed reactors by superimposing axial dispersion on plug flow (Berger et al., 2002). The ADM involves only one parameter, the axial dispersion coefficient, usually expressed as a Péclet number. The "cells in series" model considers a flow through a series of mixing cells in the interstices of the packing, where the flow is characterized by the number of cells in series and the liquid holdup. However, this model does not adequately represent the actual flow in a

* Corresponding author. Tel.: +1-314-9357187; fax: +1-314-9357211.
E-mail address: muthanna@che.wustl.edu (M. Al-Dahhan).

0009-2509/$ - see front matter © 2004 Elsevier Ltd. All rights reserved.
doi:10.1016/j.ces.2004.01.048

packed-bed (Iliuta et al., 1996). The crossflow model has been suggested to account for the considerable liquid stagnancy. It assumes that liquid holdup can be split into two parts: stagnant pockets or films, and liquid in plug flow, with exchange between the two. The cross flow model requires three parameters: the fraction of the plug flow, the exchange coefficient, and the external liquid holdup (Hochman and Effron, 1969).

It is well known that most industrially important reactions involve complex reaction kinetics, such as in the catalytic wet oxidation (CWO) of liquid-phase organics. To interpret the reaction in packed-bed reactors, one needs an assessment of the flow behavior, such as holdup and partial catalyst wetting, as well as the relative importance of the various mass transport resistances. Hence, it is important to incorporate the complexities of external mass transfer and hydrodynamics with a catalytic reaction for the entire reactor. Recently, Iliuta and Larachi (2001) have discussed the design of reactors by exploring a parallel modeling framework in which the reactor and particle scales were considered. The reactor scale piston dispersion exchange (PDE) model was employed to capture both transient and space dependences of reactants in the dynamic and static liquid zone. The mass transfer processes between gas–liquid, gas–solid, and dynamic liquid–static liquid were integrated. Chemical reaction, as a sink to deplete the reactants, was coupled with the (PDE) model. At the pellet scale, they solved the general diffusion–reaction equation to supply the time and space distribution of the reactant concentrations. They employed a parallel solution strategy to simultaneously resolve the pellet and the reactor scale model for the CWO of phenol in a packed-bed with MnO_2/CeO_2 catalyst pellets. However, no experimental observations were supplied to verify their simulation results.

In the present work, having developed a different set of governing equations, a modeling scheme that combines the reactor scale ADM with the pellet scale model is proposed. A sequential solution strategy is developed, where the ADM predicts the local concentration along the reactor axis, while the pellet scale model evaluates the local effectiveness factor corresponding to the local reactant concentration. To demonstrate the dynamic behavior, the sequential approach is applied for each time step. Correspondingly, the simulation describes the time evolution of catalyst stability at each constructed matrix cell. Before the sequential modeling scheme (this work) and the parallel modeling scheme (Iliuta and Larachi, 2001) are applied for CWO, however, they are validated via comparison between the model simulations and the experimental observations for hydrogenation of alpha-methylstyrene to cumene in hexane solvent.

2. Model development

Most of the published works on packed-bed models aim to describe the hydrodynamics of reactors in cold flow, such as hydrocarbons–nitrogen or water–air, (Iliuta et al., 1996), which are not reactive at all. However, the present work focuses on packed-bed models incorporating reactions. For the model formulation, the following reaction type is considered:

$$A(g) + v_B B(l) \rightarrow \text{Products}$$

where the gaseous species, A, reacts with the liquid species, B. The primary model variables of interest are the liquid phase concentrations of the dissolved gaseous reactant and the resulting conversion of the liquid phase reactants. Mass transfer resistances consist of two cases: the interphase resistance between the gas, liquid, and solid phases, as well as the intraparticle resistance inside the catalyst particles. The interphase mass transfer is reflected in the reactor scale model, whereas the intraparticle mass transfer is tackled via the pellet scale model.

The model development is based on several general assumptions: the gas and liquid flow rates are constant throughout the reactor; axial dispersion in the gas phase is negligible; conditions are uniform in the radial direction and maintain steady state; the concentration level of pollutant in the feed stream is so low that isothermal conditions prevail; local thermal equilibrium and mass transfer equilibrium exist between the gas and liquid phases; and no correction of effective diffusivity is made to account for progressive deactivation by carbonaceous deposits.

2.1. Reactor scale model

Considering gas and liquid in plug flow subject to the above assumptions, the plug-flow reactor scale model allows for different reaction rates on the dry and wetted pellets by considering gas–liquid and liquid–solid mass transport along with the pertinent kinetics. El-Hisnawi (1981) employed the heterogeneous plug-flow model for low-pressure operation in a trickle bed reactor to solve the gas-limited reaction problem due to externally dry catalyst areas. An overall wetting efficiency (η_{CE}) was introduced in the plug-flow model to account for the partial wetting of the catalyst particles. The key effect incorporated in such a model was that of partial wetting and transport of gaseous reactant to dry external areas of the catalyst, resulting in high rates observed in the experimental data for gas-limited reaction. The surface concentration of the limiting reactant was obtained by solution of the reaction transport equation at the catalyst surface, and then it was substituted into the plug-flow equation to obtain the profile for the non-limiting reactant along the reactor length. Analytical solutions were derived for first-order kinetics for the resulting coupled linear ordinary differential equations at low pressure.

Khadilkar et al. (1996) has employed El-Hisnawi's plug-flow model for the reaction of hydrogenation of AMS at high pressure (1.5 MPa), where a numerical solution was demanded due to non-linear kinetics exhibited by the reaction. The pellet effectiveness factor in El-Hisnawi model

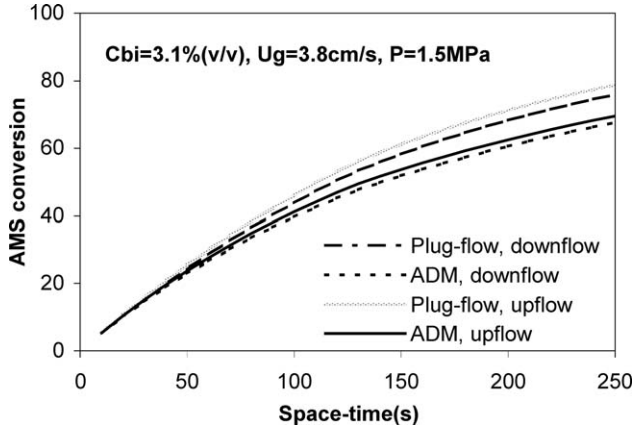

Fig. 1. The influence of axial dispersion on the conversion of alpha-methylstyrene.

was fitted at one space–time with the experimental observation. Then the effectiveness factor was used as a fitting parameter for the other space–time, which, however, in no way reflected the actual mass transfer resistance inside the pellet and the pellet external wetting contact with the liquid.

Axial dispersion can be severe in trickle flow or bubbly flow reactors with increasing conversion, reaction order, or higher eddy diffusivities, such as when conversion reaches about 90% for a laboratory scale TBR of 0.3 m in length (Mears, 1971). Several criteria have been proposed in the literature for appraising the significance of the axial dispersion effect. An early one was developed by Mears (1971) for liquid-limiting reactions based on the minimum bed-length required to neglect the axial dispersion effect. Later, based on the development of an approximate solution of the axial dispersion model, Cassanello et al. (1992) established a general criterion valid for either liquid- or gas-limited reactions. By applying the criterion to the conditions used for our test reaction of AMS hydrogenation and phenol oxidation, we found that the axial dispersion effects cannot be neglected for both cases. In addition, as exhibited in Fig. 1, significant differences were found in the conversion predictions, depending on whether the liquid phase behavior is described according to the plug flow or the axial dispersion models at relatively high space–time. For both the downflow and upflow operation conditions, the deviation of ADM from plug flow is more than 15% at low liquid superficial velocity with a space–time around 250 s. Therefore, axial dispersion can be considered significant under the employed conditions, and the ADM is applied in the following modeling scheme.

Axial dispersion is accounted for in the reactor model via the dispersion coefficient D_{EL} for the reactants A and B, as well as the product C in the liquid phase. The dispersion coefficient is obtained by assuming that all the mixing processes follow Fick's Laws. The ADM at steady state can be described as follows for all three components, A, B, and C, in the liquid phase:

Generalized governing equation for ADM:

$$D_{EL,A}\frac{d^2C_{A,L}}{dz^2} - u_{SL}\frac{dC_{A,L}}{dz} + (ka)_{GL}[C_{A,e} - C_{A,L}] - k_{LS,A}a_{LS}[C_{A,L} - C_{A,LS}] = 0, \quad (1)$$

$$D_{EL,B}\frac{d^2C_{B,L}}{dz^2} - u_{SL}\frac{dC_{B,L}}{dz} - v_B k_{GS,A}a_{GS}[C_{A,e} - C_{A,GS}] - k_{LS,B}a_{LS}[C_{B,L} - C_{B,LS}] = 0, \quad (2)$$

$$D_{EL,C}\frac{d^2C_{C,L}}{dz^2} - u_{SL}\frac{dC_{C,L}}{dz} - k_{LS,C}a_{LS}[C_{C,L} - C_{C,LS}] = 0. \quad (3)$$

Mass transfer:

$$k_{LS,m}a_{LS}[C_{m,L} - C_{m,LS}] = \eta_o(1-\varepsilon_B)\eta_{CE}r_m(C_{m,LS}), \quad m = \mathrm{A,B,C}, \quad (4)$$

$$k_{GS,A}a_{GS}[C_{A,e} - C_{A,GS}] = \eta_o(1-\varepsilon_B)(1-\eta_{CE}) \times r_A(C_{A,GS}). \quad (5)$$

Boundary conditions (*Danckwerts' type*):

$$-D_{EL,m}\frac{dC_{m,L}}{dz} = u_L[C_{m,0} - C_{m,L}], \quad m = \mathrm{A,B,C} \quad \text{at } z = 0, \quad (6)$$

$$\frac{dC_{m,L}}{dz} = 0, \quad m = \mathrm{A,B,C} \quad \text{at } z = L. \quad (7)$$

When the dispersion is dominated by molecular diffusion, the boundary conditions are of Danckwerts' type. The analysis of the construction arrangement of two-phase flow reactors suggests that the Danckwerts boundary conditions represent the best approximation of the reality for the majority of the real reactors (Iliuta et al., 1996). The above equations can be written in dimensionless form by introducing the following variables:

Let

$$\xi = \frac{z}{L}, \quad \alpha_{GL} = \frac{(ka)_{GL}L}{u_{SL}}, \quad \alpha_{GS} = \frac{k_{GS,A}a_{GS}Lv_B}{u_{SL}},$$

$$\alpha_{LS,m} = \frac{k_{LS,m}a_{LS}L}{u_{SL}}, \quad C_{A,e} = \frac{P_{A,G}}{H_A}, \quad c_{m,L} = \frac{C_{m,L}}{C_{A,e}},$$

for $m = \mathrm{A,B,C}$

$$\beta_1 = \frac{L\eta_{CE}\eta_o(1-\varepsilon_B)}{u_{SL}C_{A,e}}, \quad \beta_2 = \frac{L(1-\eta_{CE})\eta_o(1-\varepsilon_B)v_B}{u_{SL}C_{A,e}},$$

$$Pe = \frac{u_{SL}L}{D_{EL}}.$$

Substitution of the above dimensionless groups into the equations leads to the following ordinary differential equations:

Dimensionless ADM:

$$\frac{1}{Pe}\frac{d^2c_{A,L}}{d\xi^2} - \frac{dc_{A,L}}{d\xi} + \alpha_{GL}(1 - c_{A,L}) - \alpha_{LS,A}(c_{A,L} - c_{A,LS}) = 0, \quad (8)$$

$$\frac{1}{Pe}\frac{d^2c_{B,L}}{d\xi^2} - \frac{dc_{B,L}}{d\xi} - \alpha_{GS}(1 - c_{A,GS}) - \alpha_{LS,B}(c_{B,L} - c_{B,LS}) = 0, \quad (9)$$

$$\frac{1}{Pe}\frac{d^2c_{C,L}}{d\xi^2} - \frac{dc_{C,L}}{d\xi} - \alpha_{LS,C}(c_{C,L} - c_{C,LS}) = 0. \quad (10)$$

Mass balance:

$$\alpha_{LS,m}[c_{m,L} - c_{m,LS}] = \beta_1 r_m(c_{m,LS}); \quad \text{for } m = \text{A, B, C}, \quad (11)$$

$$\alpha_{GS}[1 - c_{A,GS}] = \beta_2 r_A(c_{A,GS}). \quad (12)$$

Boundary conditions:

$$\frac{1}{Pe}\frac{dc_{m,L}}{d\xi} = [c_{m,L} - c_{m,0}] \quad m = \text{A, B, C} \quad \text{at } \zeta = 0,$$

$$\frac{dc_{m,L}}{d\xi} = 0; \quad m = \text{A, B, C} \quad \text{at } \zeta = 1.0.$$

If we were to neglect the axial dispersion in the liquid, the calculations would be markedly simplified. The two-point boundary value problem would be eliminated, and the axial dispersion model would turn out to be the original plug-flow model proposed by El-Hisnawi (1981). Similar to the El-Hisnawi model, the above reactor scale ADM requires the pellet effectiveness factor, η_0, to be supplied as a known parameter. For a linear apparent kinetics expression that includes the intraparticle resistance, the Thiele modulus allows us to derive the pellet scale effectiveness factor. However, complex kinetics expressions are often found in the literature, especially when catalysts suffer from deactivation, which leads to varied reaction rates due to the loss of the catalyst active sites. In such cases, the apparent reaction kinetics expression cannot suitably predict the evolution of the reactor performance.

Pintar et al. (1997) set the value of the effectiveness factor to 1.0, assuming that the reaction rate at given reaction conditions is not influenced by internal transport resistance. Generally, however, the intraparticle diffusion resistance is significant (large Thiele modulus) and the reaction rate is large compared to the internal diffusion rate. The transport effect can be explained by the inability of the liquid reactant to diffuse rapidly enough to the zones adjacent to the dry catalyst surface where the gas reactant is abundant. Thus, the internal transport greatly affects the observed reaction rate, and the effectiveness factor has to be determined by considering the pellet scale phenomena. One of the pellet scale models was proposed by Beaudry et al. (1987) to illustrate the intraparticle diffusion–reaction process. Such a model is discussed in the next section and is employed in the present work.

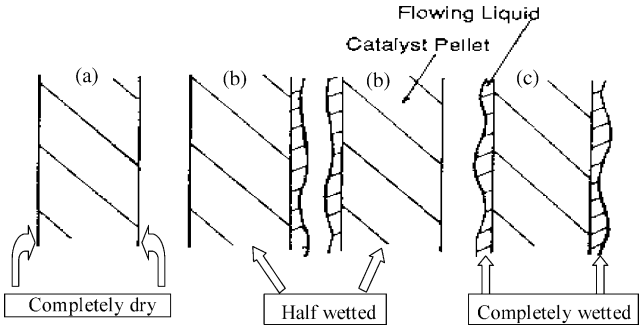

Fig. 2. Representation of possible catalyst pellet wetting contact.

2.2. Pellet scale model

Beaudry et al. (1987) described catalyst pellets in the form of infinite slabs with both sides exposed to either gas or liquid, or as a half-wetted pellet exposed to gas on one side and liquid on the other. The approach for the evaluation of the overall effectiveness factor for partially wetted catalyst particles was in line with the concept proposed by Ramachandran and Smith (1979), who considered the intraparticle diffusion as the result of contributions arising from the liquid-covered surface of the particles (based on the external wetting efficiency) and from the gas-covered surface. Accordingly, Beaudry model divided the effectiveness factor of catalyst pellets into three liquid–solid contacting categories: (a) both catalyst surfaces are completely dry, i.e., gas-covered (η_{od}); (b) one of the catalyst surfaces is actively wetted and the other one is dry (η_{odw}); (c) both catalyst surfaces are completed wetted, i.e., liquid covered (η_{ow}), as exhibited in Fig. 2. Intuitively, this approach represents the reality better than assuming that all particles have the same fraction of external wetting. The reactor-scale overall effectiveness factor, η_0, can be defined as the weighted average of η_{od}, η_{odw}, and η_{ow}, based on the general consideration of the presence of all three categories, with the corresponding weights given as $(1 - \eta_{CE})^2$, $2\eta_{CE}(1 - \eta_{CE})$, and η_{CE}^2, respectively. This way the sum of the weights turns out to be unity. The contacting efficiency, η_{CE}, is the fraction of the external catalyst surface area that is actively wetted. Therefore, the overall effectiveness factor is given as

$$\eta_o = (1 - \eta_{CE})^2\eta_{od} + 2\eta_{CE}(1 - \eta_{CE})\eta_{odw} + \eta_{CE}^2\eta_{ow}, \quad (13)$$

where η_{od}, η_{odw}, and η_{ow} are calculated as integral functions of reactant concentration along the pellet scale length based on an inactively wetted surface or an actively wetted surface. In other words, pellet reactant concentration profiles, as shown in Fig. 3, have to be available before the overall effectiveness factor can be obtained. At low pressure, the gaseous reactant supplied from both sides of the pellet is depleted completely within a short distance depending on the extent of the gas reactant limitation. The term $(1 - w_x)V_s/S_x$ shows the distance from the fully dry surface, and the term

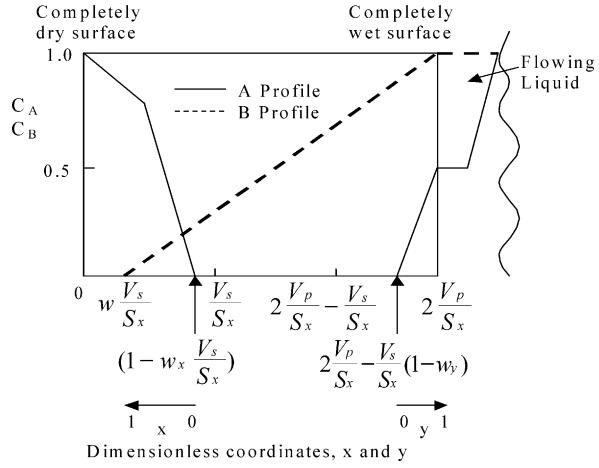

Fig. 3. Possible concentration profiles along the pellet scale at liquid reactant limiting conditions.

$(1-w_y)V_s/S_x$ shows the distance from the fully wetted surface. The distance measured from the fully dry surface to the plane where the liquid reactant depletes completely is noted as term wV_s/S_x. The above-mentioned terms are also shown in Fig. 3. The concentration distribution of reactants within the pellet was obtained via a group of dimensionless differential equations, as listed below. The details concerning derivation of the governing equations and the description of each term for a pellet scale model were reported by Beaudry et al. (1987).

Governing equations for Beaudry et al. (1987) *model*:

$$\frac{d^2c_A}{dx^2} - (1-w_x-w)^2\left(\frac{V_s}{S_x}\right)^2\frac{(-r_A)}{D_{eA}} = 0, \quad 0<x<1, \tag{14}$$

$$\frac{d^2c_B}{dx^2} - (1-w_x-w)^2\left(\frac{V_s}{S_x}\right)^2\frac{(-r_B)}{D_{eB}} = 0, \quad 0<x<1, \tag{15}$$

$$\frac{d^2c_A}{dy^2} - (1-w_y)^2\left(\frac{V_s}{S_x}\right)^2\frac{(-r_A)}{D_{eA}} = 0, \quad 0<y<1, \tag{16}$$

$$\frac{d^2c_B}{dy^2} - (1-w_y)^2\left(\frac{V_s}{S_x}\right)^2\frac{(-r_B)}{D_{eB}} = 0, \quad 0<y<1. \tag{17}$$

Boundary conditions:

$$\left.\frac{dc_A}{dy}\right|_{y=1} = (2-w)Bi_{ls,A}(c_{A,L}-c_A|_{y=1}),$$

$$\left.\frac{dc_B}{dy}\right|_{y=1} = (2-w)Bi_{ls,B}(c_{B,L}-c_B|_{y=1}),$$

$$\left.\frac{dc_A}{dx}\right|_{x=1} = \frac{1-w_x-w}{w+1/Bi_{gs,A}}(c_{A,L}-c_A|_{x=1}),$$

$$c_A|_{x=0} = c_A|_{y=0} - 2\left(\frac{v_p}{v_s}-1\right)\left.\frac{dc_A}{dy}\right|_{y=0},$$

$$c_B|_{x=1} = 0, \quad \left.\frac{dc_B}{dx}\right|_{y=0} = 0,$$

$$\left.\frac{dc_A}{dx}\right|_{x=0} = -\frac{1-w_x-w}{1-w_y}\left.\frac{dc_A}{dy}\right|_{y=0},$$

$$\left.\frac{dc_B}{dx}\right|_{x=0} = -\frac{1-w_x-w}{1-w_y}\left.\frac{dc_B}{dy}\right|_{y=0},$$

$$c_B|_{x=0} = c_B|_{y=0} - \frac{2(v_p/v_s-1)+w_x+w_y}{1-w_y}\left.\frac{dc_B}{dy}\right|_{y=0},$$

where $Bi=(kV_s)/(D_{EL}S_x)$, $c_{m,L}=C_{m,L}/C_{A,e}$ for $m=\mathrm{A,B}$.

The boundary conditions listed above are based on the reactant concentrations in the reactor liquid phase, which have to be calculated from the reactor scale model. By assuming the concentration of gas reactant dissolved in the liquid phase changes very little due to the slight solubility of gas, Beaudry et al. (1987) replaced the dimensionless liquid concentration c_{AL} by unity and used the reaction with linear reaction kinetics at low pressure (gas-limited conditions). Analytical solutions for reactor outlet conversion have been derived for the outlet conversion of the non-volatile reactant by substituting the overall effectiveness factor into a reactor scale plug-flow model, which did not account for the interphase mass transfer.

The catalyst effectiveness factor addressed so far is only for simple linear kinetics under isothermal conditions. Several issues still remain unresolved at this stage. Most of the important reactions represent the complex consecutive/parallel reaction pathway described by Langmuir–Hinshelwood kinetics (Pintar and Levec, 1994). In addition, the assumption that the concentration of gas reactant dissolved in the liquid phase changes very little can hardly be supported from a practical point of view (Pintar et al., 1997). The knowledge of reactant concentration in the liquid bulk phase is still necessary to define the boundary conditions for the pellet-scale model.

Khadilkar et al. (1996) explored the Beaudry model for the non-linear reaction rate of hydrogenation of AMS at high pressure (1.5 MPa), which demands the numerical solution of the reaction–diffusion equations (Eqs. (14)–(17)). In their approach, pellet scale equations were solved for a range of selected bulk liquid reaction concentrations given as the boundary conditions. Then the pellet effectiveness factor was fitted as a polynomial function of bulk concentrations. This polynomial was then used at each space–time to solve the reactor scale plug-flow equations originally proposed by Beaudry et al. (1987).

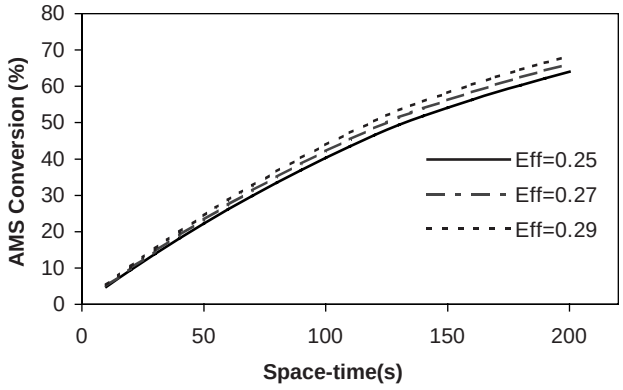

Fig. 4. Sensitivity of ADM to the effectiveness factor for hydrogenation of AMS. $P = 1.5$ MPa, downflow, $C_{AMS,0} = 3.8\%$ (v/v), $u_g = 3.8$ cm/s.

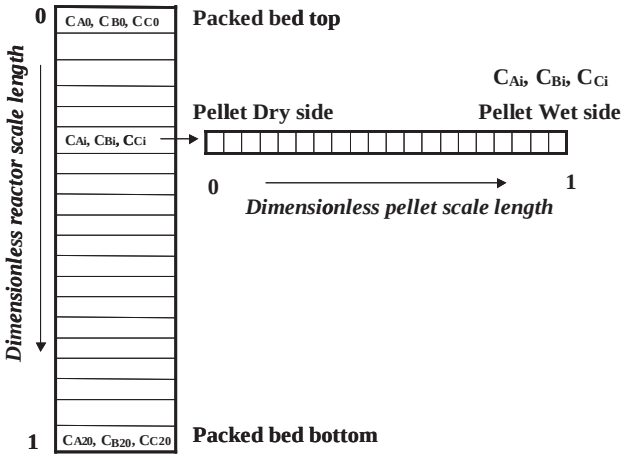

Fig. 5. Configuration of matrix cell based on the discretization of reactor and pellet scale.

However, polynomial fitting is still an approximation process, which may be not possible when one wants to derive a polynomial from the concentrations of multi-component reactants. In addition, when catalyst deactivation occurs, the loss of the catalyst active sites leads to a dynamic reaction rate. Thus, the reactant concentrations in the liquid bulk and on the catalyst surface keep changing, which makes the fitted polynomial derivation not feasible. The fitting error may lead to significant deviation for the pellet overall effectiveness factor, η_o, and hence, noticeable error in the reactor scale simulation results. In this work, the sensitivity of the ADM to the parameter η_o has been tested by predicting the AMS conversion based on different values of effectiveness factor for the whole reactor, as shown in Fig. 4. It is confirmed that changing the parameter η_o leads to considerable deviation from the reactor scale model simulation.

The overall effectiveness factor is varied at each axial location, and the range of its variation is significant. Thus, in this work, the developed computational scheme allows us to calculate the values of the effectiveness factor directly from the pellet scale model for a given time at each axial reactor location. We can thereby get a local effectiveness factor corresponding to the local reactant concentrations, instead of the one obtained from polynomial fitting.

2.3. Computational scheme: sequential approach

In this work, the performance of a packed-bed over a range of operating conditions has been investigated by using the ADM in combination with the pellet scale model. At first the ADM (Eqs. (8)–(12)) is solved with an initial value of the pellet overall effectiveness factor to predict the profile of local concentrations along the reactor axis, such as the reactant concentrations at the liquid bulk phase and on the catalyst surface. Once the local reactant concentrations at each reactor collocation point are known, the corresponding boundary conditions for the pellet scale model become available. Accordingly, the pellet scale model (Eqs. (14)–(17)) is solved to evaluate the overall effectiveness factor (Eq. (13)) at every axial collocation point. Then the newly obtained set of pellet overall effectiveness factors are used again as the input to the ADM, where the local reactant concentrations along the reactor axis are updated. The newly obtained local reactant concentrations are employed to compute the overall effectiveness factor at every axial collocation point. These steps are iterated until convergence is achieved, when the latest values of the pellet overall effectiveness factors along all the reactor axial collocations adequately match the ones used in the previous iteration. It is noteworthy that no adjustable parameters have been used in this proposed sequential approach.

Both the reactor scale ADM and the pellet scale model involve coupled non-linear ordinary differential equations. Correspondingly, both of them demand a numerical solution due to the incorporation of the non-linear reaction rate expression. Hence, on the basis of the orthogonal collocation method, a FORTRAN program using the subroutine COLDAE was developed to solve the coupled non-linear ODE with algebraic constraints. Orthogonal collocations are known as a robust method for solving boundary value problems (Villadsen and Michelsen, 1978). Twenty-one collocation points are specified for both reactors and catalyst pellets, in order to set up a matrix configuration with one dimension for the reactor scale from inlet to outlet and the other dimension for the pellet scale from the side covered by gas (fully dry) to the side covered by liquid (fully wet), as shown in Fig. 5. Thus, the local information at each cell, including component concentrations and effectiveness factors, can be computed numerically.

When catalyst deactivation exists, the solution is more complicated due to the dynamic behavior of the catalyst. The reaction investigated in this work is the catalytic oxidation of phenol over a deactivating catalyst. Both the intrinsic reaction rates and the loss rate of the catalyst active site fraction are given as functions of the catalyst active site fraction and of the reactant and product concentrations in

the liquid bulk. Details of the kinetics will be discussed in a later section. The computational scheme presented above is designed for the reactor and pellet at steady state conditions. To consider the dynamic problem, in which the catalysts deactivate as the time progresses, the time scale needs to be incorporated. Correspondingly, upwind discretization of the time dimension is carried out in constant steps to divide the reaction duration into a series of time zones. The solution scheme starts with time equal to zero, with the initial condition given as unity for the catalyst active site fraction, so that the initial intrinsic reaction rates are simplified to the function of reactant concentrations in the liquid bulk. The proposed sequential scheme of the combination of reactor- and pellet-scale models is now applicable to obtain the local concentration distribution for the initial time point. Based on the obtained local concentrations, a small value of the time step is chosen so that the catalyst deactivation rate at each matrix cell during that time step can be calculated. Hence, after the time proceeds to the next preset point, the catalyst active site fraction at each cell is available, and the intrinsic reaction rates, once again, become the functions of the unknown variables of the local concentrations. Therefore, at this preset time point, the proposed sequential scheme is employed again for calculating the local concentrations. This way the local information at the specified cell and the specified time, including the species concentration and catalyst active site fraction, can be captured and the dynamic performance of packed bed and catalyst pellet can be depicted.

2.4. Mass transfer coefficients and hydrodynamic parameters

Reaction kinetics and transport dynamics are closely interlinked, and their effects on the reactant conversions are inseparable. Therefore, to properly know the behavior of the packed-bed reactors, hydrodynamic parameters are important and need to be considered. These include the degree of catalyst wetting, the mixing and flow pattern of the fluids, the axial dispersion coefficient, and the liquid holdup. The selection of hydrodynamic conditions depends not only on the processing requirement, but also on the contacting pattern. As shown in Fig. 6, the nature of multiphase contacting in various flow modes (cocurrent upflow or concurrent downflow) is distinct. When the bed is operated in the trickle flow regime under partial wetting conditions for the pellets, gas is the continuous phase and liquid is the dispersed phase. However, the packed-bubble column operates in the bubbly flow regime with fully wetted pellets. In this regime, the solid particles are wetted by the continuous liquid phase, whereas the gas phase is dispersed as bubbles flowing through the packing channels. The key differences in modeling downflow and upflow modes are the values of the mass transfer parameters and the catalyst wetting efficiency. Since upflow operation is characterized by high liquid holdups, it was assumed external wetting is complete. Table 1 lists various correlations in the literature used to calculate the model parameters, which include the external liquid–solid contacting efficiency, liquid holdup, mass transfer coefficients ($(ka)_{GL}, k_{LS}, k_{GS}$), and the axial dispersion coefficient.

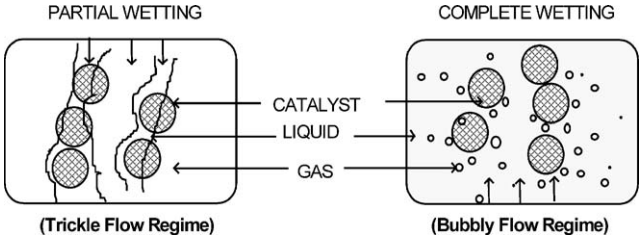

Fig. 6. Contacting pattern in the trickle flow regime and bubble flow regime.

3. Results and discussion

Many experimental investigations in the literature have dealt with hydrogenation or oxidation in moderately concentrated organic solutions or solutions with a large excess of liquid reactants. To validate the proposed model scheme, the hydrogenation of AMS to cumene in hexane solvent was taken as a model reaction. We sought to compare the simulation results with the experimental observations taken

Table 1
Summary of various correlations used in the models

Model parameter	Reference for trickle bed	Reference for bubble flow column
Gas–liquid mass transfer coefficient, $(ka)_{GL}$	Fukushima and Kusaka (1977a)	Reiss (1967)
Liquid–solid mass transfer coefficient, k_{LS}	Tan and Smith (1980)	Specchia (1978)
Gas–solid mass transfer coefficient, k_{GS}	Dwivedi and Upadhyah (1977)	0.0
Wetting efficiency, η_{CE}	El-Hisnawi (1981)	1.0
Axial dispersion coefficient	Cassanello et al. (1992)	Cassanello et al. (1992)
Liquid holdup, ε_L	Fukushima and Kusaka (1977b)	Bensetiti et al. (1997)

Table 2
Design and operating conditions

Property	Hydrogenation of AMS	CWO of phenol
Temperature (°C)	25	80
Pressure (MPa)	0.3–1.5	0.5
Reactor diameter (cm)	2.2	5.1
Bed height (cm)	27.5	200
Bed porosity	0.40	0.36
Catalyst particle size (cm)	$\phi 0.13 \times 0.56$	$\phi 0.3$
Density of catalyst particle (kg/m^3)	1222	1760
Superficial liquid velocity (cm/s)	0.09–0.5	0.1–0.22
Superficial gas velocity (cm/s)	3.8–14.4	1.0–10.5
Feed concentration (mol/l)	0.23–0.60, (3.1–7.8% (v/v))	0.001–0.03

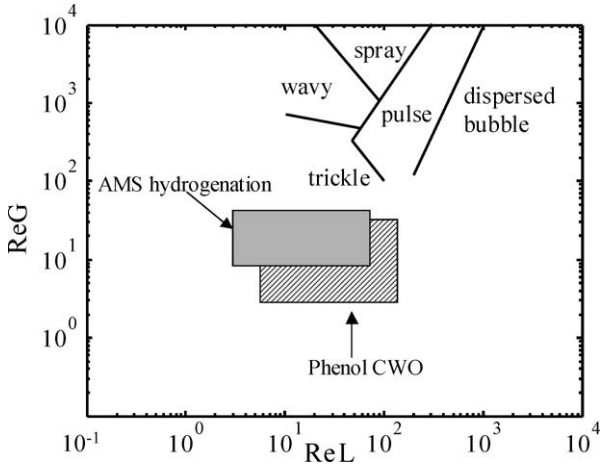

Fig. 7. Region of trickle flow regime covered experimentally in this work for AMS hydrogenation and phenol oxidation, (flow map proposed by Fukushima and Kusaka (1977b)).

from Khadilkar et al. (1996). Then the reaction of aqueous phenol oxidation, which is of our interest, was applied to the proposed model to predict the performance of the reactor and catalyst pellet under different operating conditions. The employed design parameters of the three-phase reactors, the characteristics of the porous catalyst particles, and the operating conditions are indicated in Table 2. The trickle flow regime experimentally covered in this work for these two reactions is shown in Fig. 7.

3.1. Model scheme validation

In the liquid phase, both hydrogen and AMS have low concentrations, which make the effect of the reaction heat release insignificant. The intrinsic kinetics expression of hydrogenation of AMS has been studied by Khadilkar et al. (1996), who fitted separate Langmuir–Hinshelwood rate expressions (Eq. (18)) for different pressures:

$$r_B\left[\frac{\text{mol}}{\text{m}^3\text{s}}\right] = \frac{k_{vs}C_{\alpha ms}C_{H2}}{(1+K_1C_{\alpha ms}+K_2C_{cume})^{\beta}}. \quad (18)$$

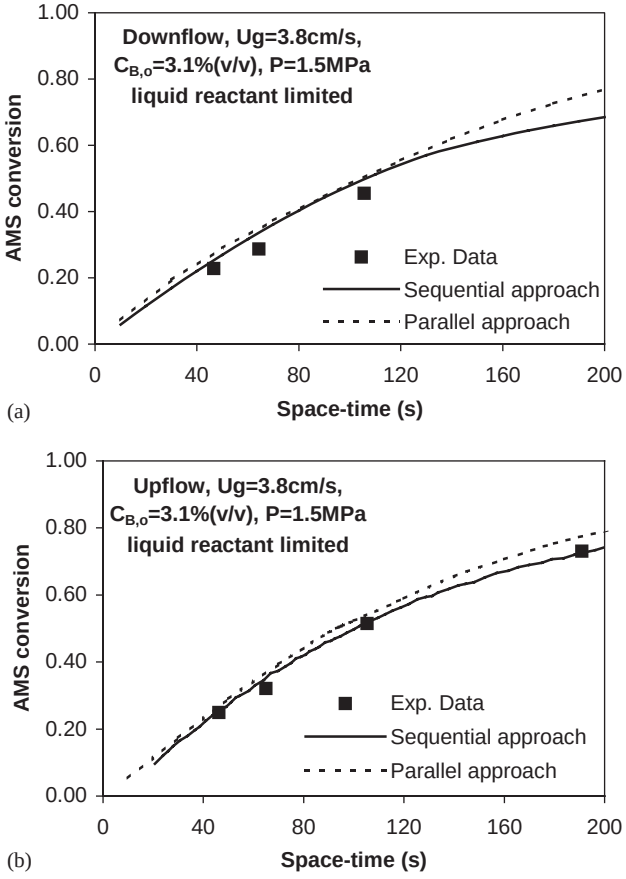

Fig. 8. (a) Downflow and (b) upflow performance at high pressure: experimental data and model predictions. The curves correspond with the predictions via parallel approach proposed by Larachi et al. (2001) and the one via sequential approach proposed in this work.

According to the taxonomy (Khadilkar et al., 1996), the ratio of the diffusion fluxes of the two reactants ($\gamma = (D_{eB}C_{Bi}/v_B(D_{eA}C_A^*)$) is indicative of the relative availability of the species at the reaction site. The reaction can be considered gas reactant limited for $\gamma \gg 1$ or liquid reactant limited for $\gamma < 1$. At high pressure (1.5 MPa) and a low feed concentration of AMS ($C_{B,0} = 3.1\%$, v/v), the reaction is liquid limited ($\gamma < 1$), such as in Fig. 8a and b, where

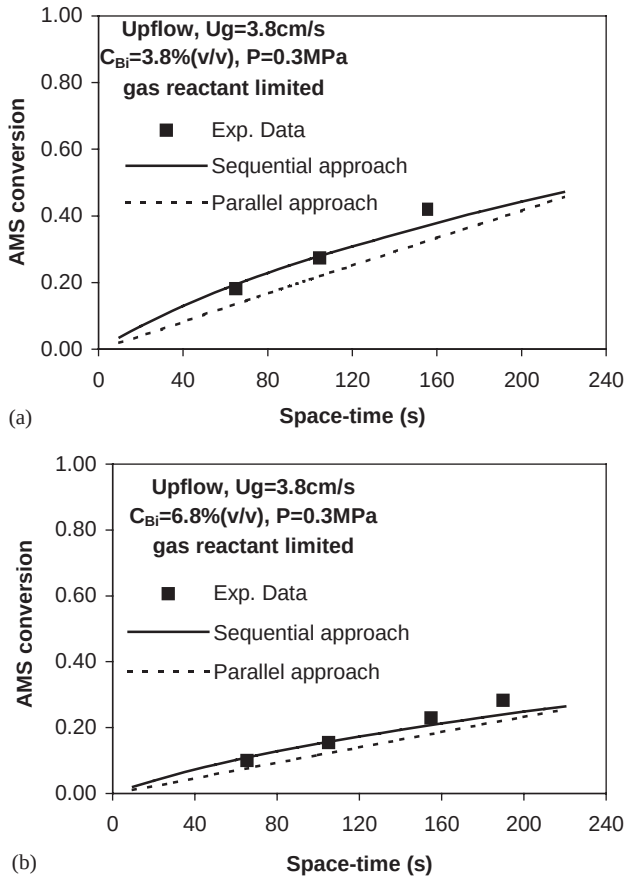

Fig. 9. Effect of feed concentration on upflow performance: experimental data and model predictions.

the effect of the flow direction on reactor performance is shown. As pressure is decreased from 1.5 to 0.3 MPa, and feed concentration of AMS is increased to $C_{B,0} = 6.8\%$ (v/v), the reaction is transformed to a gas-limited regime ($\gamma > 1$), such as in Fig. 9a and b, where the effect of feed concentration on upflow performance is shown.

The curves in Figs. 8 and 9 correspond with the predictions of the sequential approach proposed in this work and the parallel approach proposed by Iliuta and Larachi (2001). The two approaches contain different sets of transport and hydrodynamic correlations. In all the exhibited cases, the results predicted by both approaches agree reasonably with the experimental observations. In the parallel approach, the external liquid holdup is divided into static and dynamic portions. For high flow rates, such division is reasonable. However, the dynamic liquid holdup decreases with decreasing liquid flow rate, i.e., when the liquid space–time increases (Iliuta et al., 1996). When the liquid space–time reaches 200 s, the liquid flow rate is so low that the discrepancy between the dynamic and static liquid holdup is no longer distinct, which means the split-up of the external holdup is not necessary. Nevertheless, the parallel approach always assumes there is a difference between these two portions. Hence, for the liquid-limited reaction in Fig. 8a and b, the deviation between these two approaches becomes larger as the space–time increases. Such deviation is not shown for the gas-limited reaction in Fig. 9a and b, where both the liquid holdup and the gas pressure can affect the AMS conversion.

Since the suitability of the sequential approach to describe the reactions in packed-bed has been validated, it is applied to the other test case, which is the CWO of phenol over a deactivating catalyst.

3.2. Wet air oxidation of aqueous phenol

Catalyst deactivation was overlooked in most of those investigations dealing with CWO, which has focused on the evaluation of catalyst performance in terms of the removal rate of pollutant with simplified or complex rate equations (Levec and Smith, 1976, Maugans and Akgerman, 2003). In fact, catalyst deactivation occurs in general cases due to the polymer deposition on the catalyst surface, or due to the leaching of the catalyst active sites. Hence, the time variable also needs to be taken into account to describe dynamic catalytic behavior. Although catalyst deactivation due to active ingredient leaching out in the hot acidic reaction media is documented (Pintar and Levec, 1992), the activity loss due to the carbon deposits on catalyst surface has been mostly discounted. Hamoudi et al. (1999), who studied phenol oxidation in a slurry reactor over a newly developed but rapidly deactivated MnO_2/CeO_2 catalyst, have reported that oxidative coupling reactions contribute significantly to rapid catalyst deactivation via coke deposition on the surface of catalyst pellets. Relatively few reports have been published on modeling a packed-bed reactor for a multi-step complex reaction system with such a deactivating catalyst.

3.2.1. Intrinsic kinetic model

In this evaluation of wet air oxidation of aqueous phenol in packed-beds, the reaction proceeds between phenol and an excess of soluble oxygen in the presence of a deactivating MnO_2/CeO_2 mixed oxide catalyst. The complete multiple deactivation-reaction network describing phenol CWO has been reported by Hamoudi et al. (1999), in which all the intervening species are grouped into four lumps. Chemical phenol (lump B) is oxidized by O_2 and converts into a chemisorbed aqueous breakdown intermediate lump (C) that further degrades into an oxidation end-product lump D (total inorganic carbon). All three lumped species can instantaneously adsorb or desorb. A Langmuir–Hinshelwood kinetic model based on this deactivation-reaction network was proposed to predict the reaction rate of the various carbon lumps as well as the rate of decline of catalyst activity. The kinetic model and its calculated parameters successfully described the time course of the four carbon lumping species involved in the slurry reaction (Hamoudi et al., 1999).

$$r_B \left[\frac{\text{mol}}{\text{kgcat min}}\right] = \frac{k_2 K_1 \varphi C_{BL}}{1 + K_1 C_{BL} + K_3 C_{CL} + K_3' C_{DL}},$$

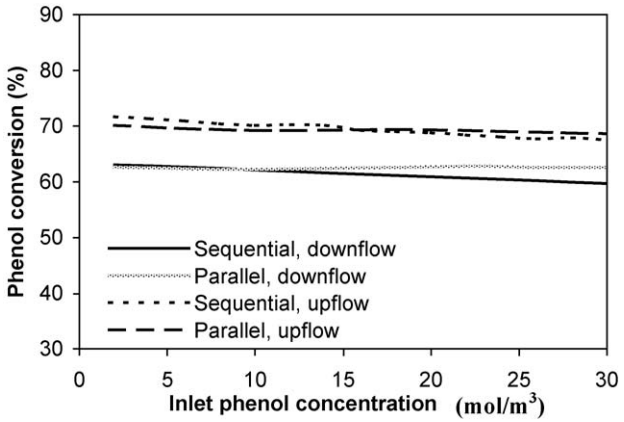

Fig. 10. Effect of inlet phenol concentration on phenol conversion in fixed bed reactors, time = 5 h, $u_{SL} = 0.15$ cm/s, $u_g = 2.8$ cm/s, $P = 0.5$ MPa, $T = 80°C$.

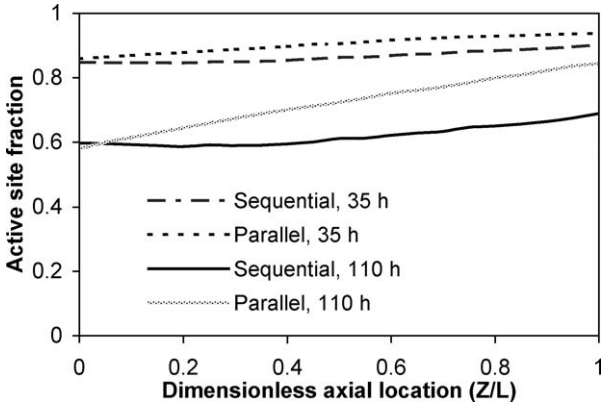

Fig. 11. Comparison of axial distribution of active site, downflow, time = 35 and 110 h, $C_{B,0} = 6$ mol/m^3, pellet fully wet side.

$$r_C \left[\frac{\text{mol}}{\text{kgcat min}}\right] = \frac{(k_2 K_1 C_{BL} - k_2' K_3 C_{CL})\varphi}{1 + K_1 C_{BL} + K_3 C_{CL} + K_3' C_{DL}},$$

$$-\frac{\mathrm{d}\varphi}{\mathrm{d}t} = \frac{(k_4 K_1 C_{BL} + k_4' K_3 C_{CL})\varphi}{1 + K_1 C_{BL} + K_3 C_{CL} + K_3' C_{DL}},$$

where φ is the catalyst active site fraction with the initial condition given as $\varphi = 1$ at time $t = 0$. Computation of γ results in $\gamma < 1$ for the CWO operating conditions employed in Table 2. Hence the wet air oxidation in this study is a liquid-reactant limited reaction. The assumption of an isothermal condition is justified because the low phenol concentration in the liquid-phase solution results in insignificant heat generation. Because of the relatively small phenol concentration, the physical properties of water are used for the liquid phase. Under the mild operating conditions, the fugacity and activity for oxygen and water are assigned unity values. The diffusivities of phenol and oxygen and values of viscosities and densities for water at the operating conditions were estimated from the literature correlations (Reid et al., 1986)

3.2.2. Comparison of trickle bed and packed bubble flow reactor performance

In Figs. 10 and 11, both the sequential approach and the parallel approach have been employed to predict the phenol oxidation reaction. The difference in exit phenol conversion calculated by the two approaches is within 6%, as shown in Fig. 10. The sequential and parallel approaches can also be compared for their ability to predict catalyst deactivation. As evident in Fig. 11, at identical simulation conditions, calculated profiles of the activity function of catalyst in the operation time range 0–35 h exhibited a maximum relative error of 6% between the two approaches. The maximum relative error of 20% was reached after a rather long operation time (110 h). Both of the maximum relative errors were obtained at the reactor outlet. Such prediction difference between the two approaches for the catalyst deactivation can be attributed to the correspondingly different concentration profiles. For downflow operation with identical inlet conditions, as exhibited for AMS hydrogenation in Fig. 8a and b, a more noticeable difference between the concentration profiles predicted by the two approaches results from the longer residence time of reactants in the packed bed. Similarly, for the case of CWO in Fig. 11, the differences between the concentration predictions by the two approaches also become larger with the longer residence time. Such concentration differences in turn lead to the different predictions of catalyst active site fraction, which displays the maximum difference at the reactor outlet. Nevertheless, comparing two time durations such as 35 and 110 h, the trends captured by the two approaches are always similar. Taking into account the long process duration, the distinct model type and correlations used to describe the flow field, and the different methods used for the parameters' estimation, this comparison between the two approaches is still satisfying. In Figs. 10 and 11, the curves obtained by the parallel approach simulation are similar to those reported by Larachi et al. (2001).

In Fig. 10, the comparison of downflow and upflow packed-bed performances is achieved by studying phenol conversion at identical operating conditions after the catalyst has been used for 5 h. Fig. 10 also shows that the exit phenol conversion in upflow mode was 10% higher than in the downflow mode, regardless of the feed phenol concentration. In a liquid-limited reaction, the conversion will be governed by the degree of catalyst wetting. Since upflow has higher external wetting efficiency (100%) than downflow, it will facilitate the transport of the liquid reactant to the catalyst and enhance the reaction rate. This finding is in line with the case of AMS hydrogenation, where both experimental observation (Khadilkar et al., 1996) and model simulations (this work) show that an upflow reactor should be preferred for liquid-limited reactions.

To make the comparison in Figs. 12–14 between downflow and upflow more meaningful, the dimensionless reactor length axis point 0 corresponds to the packed-bed inlet, and 1 corresponds to the packed-bed outlet. Since the sequential

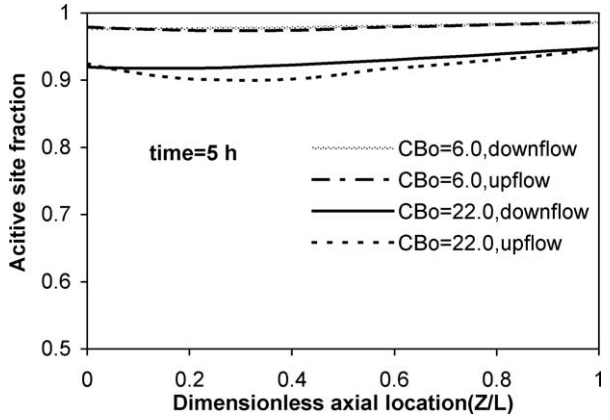

Fig. 12. Effect of inlet phenol concentration on the catalyst surface deactivation in the upflow and downflow packed-beds, $u_{SL} = 0.15$ cm/s, $u_g = 2.8$ cm/s, pellet fully wet side.

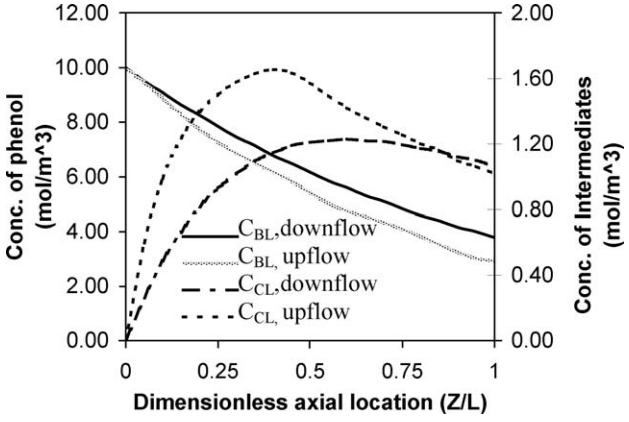

Fig. 13. Predicted concentration profiles for phenol (C_{BL}) and intermediate lump (C_{CL}) in liquid phase as a function of catalyst bed length, $u_{SL} = 0.15$ cm/s, $u_g = 2.8$ cm/s, $C_{B,0} = 10.0$ mol/m^3, $P = 0.5$ MPa, pellet fully wet side.

approach performs equivalently as the parallel approach in the validation of AMS hydrogenation, the former is used for the following evaluations. Although upflow mode will produce higher phenol conversion than downflow mode, this achievement is at the expense of more severe catalyst deactivation, as shown in Fig. 12. When the inlet phenol concentration is 6 mol/m^3, the catalyst activity loss is more in upflow than in downflow after 5 h operation, although the discrepancy is very small. When the inlet phenol concentration increases up to 22 mol/m^3, the upflow mode will do more appreciable harm to catalyst activity than downflow mode after 5 h operation. This is clear since the high phenol concentration will result in high oxidation intermediate lump concentration, and both concentrations will enhance the deactivation rate. In contrast, the effect of phenol feed concentration on conversion is not significant, as shown in Fig. 10. When the inlet concentration increases by 14 times, the change in conversion is within 6% in both upflow and downflow.

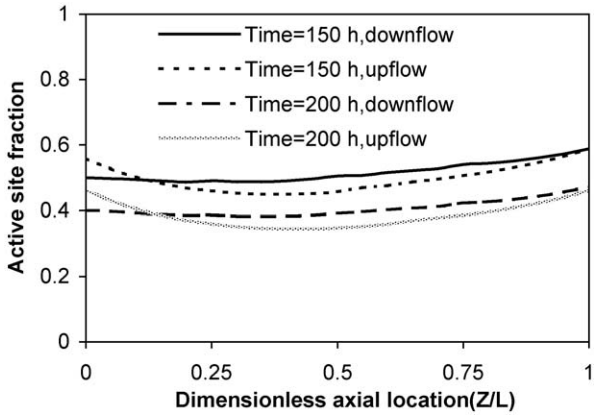

Fig. 14. Catalyst surface deactivation with time in the upflow and downflow packed-beds, $u_{SL} = 0.15$ cm/s, $u_g = 2.8$ cm/s, $C_{B,0} = 6.0$ mol/m^3, pellet fully wet side.

Since both phenol and the oxidation intermediate lump determine the rate of catalyst deactivation, we have to consider their effects simultaneously. Fig. 13 exhibits typical species concentration profiles along the packed-bed reactor at the given operating conditions after 5 h operation. Along the axis, phenol is consumed, so its concentration keeps decreasing. However, the oxidation intermediate C builds up in the first part of the reactor. With the consumption of phenol and increasing amount of C, the reaction rate of C will become negative, which can be shown from its reaction rate expression, where the concentration of C inhibits its production rate. Thus, concentration of intermediate C reaches a maximum value before the reactor outlet. At a given axial location in upflow mode, such as the middle of the reactor, the phenol concentration profile is lower than the one in downflow mode by 8%, while the concentration of product C at the same location in upflow is 22% higher than in downflow mode. Thus, when upflow mode is used, although phenol contributes less to the deactivation function, product C's contribution goes up and overtakes phenol's effect on the deactivation function. The rate of activity loss in upflow is still more than in downflow mode, which leads to the lower activity fraction profile.

The prediction of catalyst activity over time is instructive because one can learn the catalyst life expectancy, after which "coked" catalyst should be subject to burn-off and regeneration for long-term exploitation. Simulated axial profiles of activity site fraction in the time range of 0–200 h indicate the expected feature of time-declining activity, as shown in Fig. 14 for the trickle-bed operation. The simulation for the upflow reactor follows the same trend, although the upflow results in higher catalyst deactivation than the downflow. It can be expected that the majority of catalyst would completely lose its function after 300 h of operation. Although the wet oxidation of phenol over this kind of catalyst removed phenol remarkably fast at mild pressure and temperature, the catalyst underwent severe deactivation, which made its wide application undesirable. Hence,

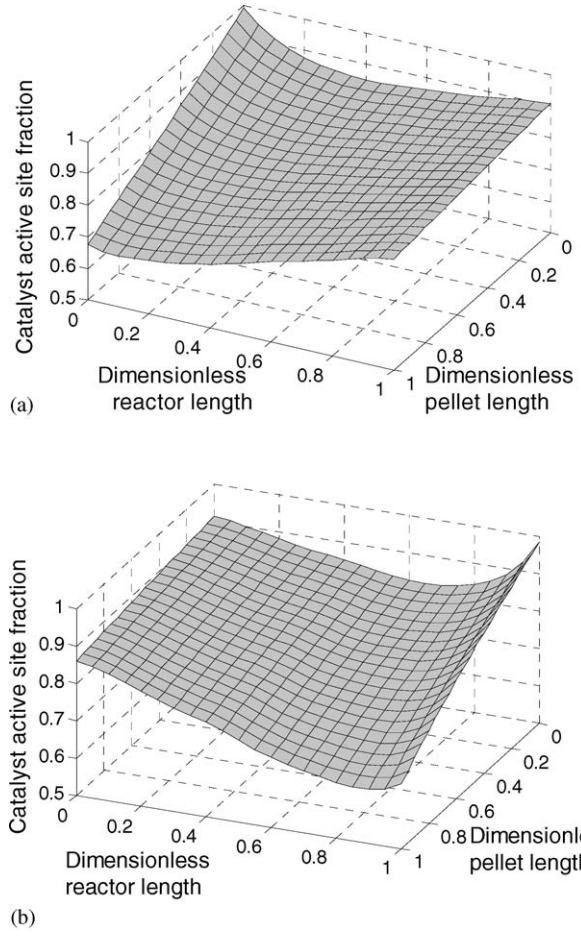

Fig. 15. Distribution of catalyst active site fraction in (a) TBR and (b) PBC, according to the proposed matrix configuration, time = 110 h, $C_{B,0} = 6.0$ mol/m^3, $P = 0.5$ MPa, $T = 80$°C.

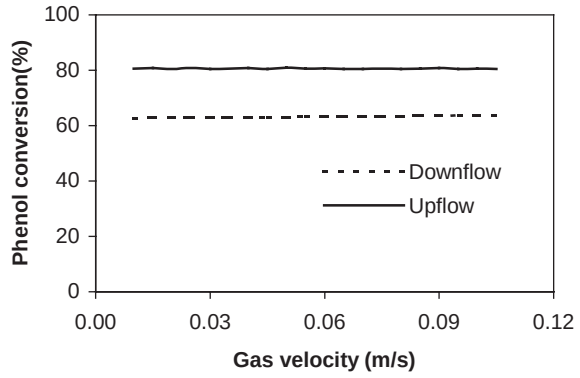

Fig. 16. Comparison of effect of gas velocity on the exit phenol conversion, upflow and downflow, $u_{SL} = 0.15$ cm/s, $C_{B,0} = 6.0$ mol/m^3, time = 5 h.

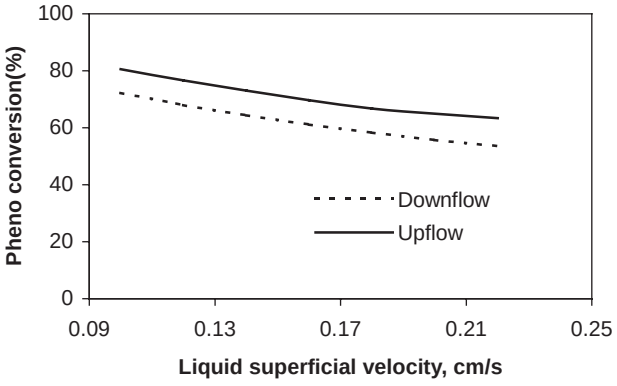

Fig. 17. Effect of liquid superficial velocity on the exit phenol conversion, upflow and downflow, $u_g = 2.8$ cm/s, $C_{B,0} = 6.0$ mol/m^3, time = 5 h.

a different catalyst is required for feasible CWO of aqueous phenol, such as the Al–Fe pillared clay catalyst (Guo and Al-Dahhan, 2003).

Both phenol conversion and catalyst deactivation should be taken into consideration when one needs to choose between upflow and downflow operation. Upflow could result in both higher phenol conversion and a higher catalyst activity loss rate, especially for wastewater that contains a high concentration of phenol. The balance between these two factors will decide the operation mode, and the catalyst's life and regeneration cycle need to be taken into account as important factors. This point is decisive in the design and selection of the three-phase reactor type for hosting the CWO.

As described in the computation scheme for the dynamic behavior, the local information at each matrix cell, such as catalyst active site fractions, is shown in Fig. 15a for the trickle bed and Fig. 15b for the packed-bed bubble column. Such information can illuminate the details of the physical phenomena inside the reactor and pellet at different operation conditions. Note that in Fig. 15a and b the dimensionless reactor length axis point 0 corresponds to the packed-bed top, and 1 corresponds to the packed-bed bottom.

3.2.3. *Influence of liquid and gas superficial velocity*

The effect of gas velocity on phenol conversion is shown in Fig. 16 for both downflow and upflow operations. Because the gas is only barely soluble, increasing the velocity has little effect on phenol conversion, even though increasing velocity will lead to an increase in the external gas–liquid mass transfer coefficients (Stuber et al., 1996). Such a negligible influence of gas velocity has earlier been observed by Goto and Smith (1975) for the oxidation of formic acid.

The comparison of effect of liquid superficial velocity on the exit phenol conversion is shown in Fig. 17 for both downflow and upflow modes. The effect of liquid superficial velocity on the axial phenol conversion profile is obvious. A lower feed flow rate is preferred because the longer residence time will allow for higher phenol conversion. A similar trend of simulation results can be obtained in the cocurrent upflow packed-bed reactor where gas flows through the liquid in bubble flow. Although a high liquid

superficial velocity enhances the mass transfer coefficient, it actually lowers the liquid reactant residence time, which corresponds to the decreased exit conversion. Such a behavior confirms that liquid reactant limiting behavior is observed for the CWO reaction, as the flow regime has already implied. Thus, the external mass transfer coefficients are dependent mostly on the liquid velocity in the downflow and upflow mode, which is in line with the model simulation and experimental verification for the hydrogenation of 2,4-dinitrotoluene (DNT) in a trickle bed (Rajashekharam et al., 1998).

3.2.4. Sensitivity of model to mass transfer coefficients

In this modeling work, a group of correlations were employed to predict the hydrodynamic parameters and interphase mass transfer resistance. However, the values of mass transfer coefficients predicted from different correlations sometimes may be dramatically different (Lemcoff et al., 1988). Thus, it is necessary to evaluate the reliability and sensitivity of model predictions to various parameters. The sensitivity of TBR models with respect to external mass transfer resistances was studied theoretically by Toppinen et al. (1996) and Rajashekharam et al. (1998). In their work, an increase or decrease in the mass transfer coefficient of up to 10 times the original estimated values results in remarkably different simulation results. Thus, the mass transfer coefficients listed in Table 1 have also been scaled up or down to investigate the sensitivity of the proposed reactor models to the mass transfer coefficients.

The effect of liquid–solid's mass transfer on the exit conversion is shown in Fig. 18a, which indicates that its influence of on phenol conversion is significant. An increase in the value of k_{LS} by 10 times improved the phenol conversion by 9%. Also, when the k_{LS} value was decreased by 10 times, the phenol conversion decreased by approximately 22%. Clearly, the liquid–solid mass transfer resistance is a important factor. Similarly, the effect of gas–liquid mass transfer on the exit conversion is shown in Fig. 18b. The results show that an increase or decrease in the $(ka)_{GL}$ value by 10 times does not substantially change phenol conversion. The insignificant difference in phenol conversion was maintained over the entire range of liquid velocity. The sensitivity of the model with respect to the gas–solid mass transfer coefficient is shown in Fig. 18c, which was obtained by increasing and decreasing the value of k_{GS} by 10 times. All three curves almost fall into the same line, which evidences the model is insensitive to the gas–solid mass transfer coefficient over the investigated range of liquid flowrates.

Hence, the liquid-reaction-limited characteristic of CWO is proved once more, and the relative importance of mass transfer resistance on the exit phenol conversion for the CWO process is liquid–solid k_{LS} > gas–liquid $(ka)_{GL} \approx$ gas–solid k_{GS}, in descending order.

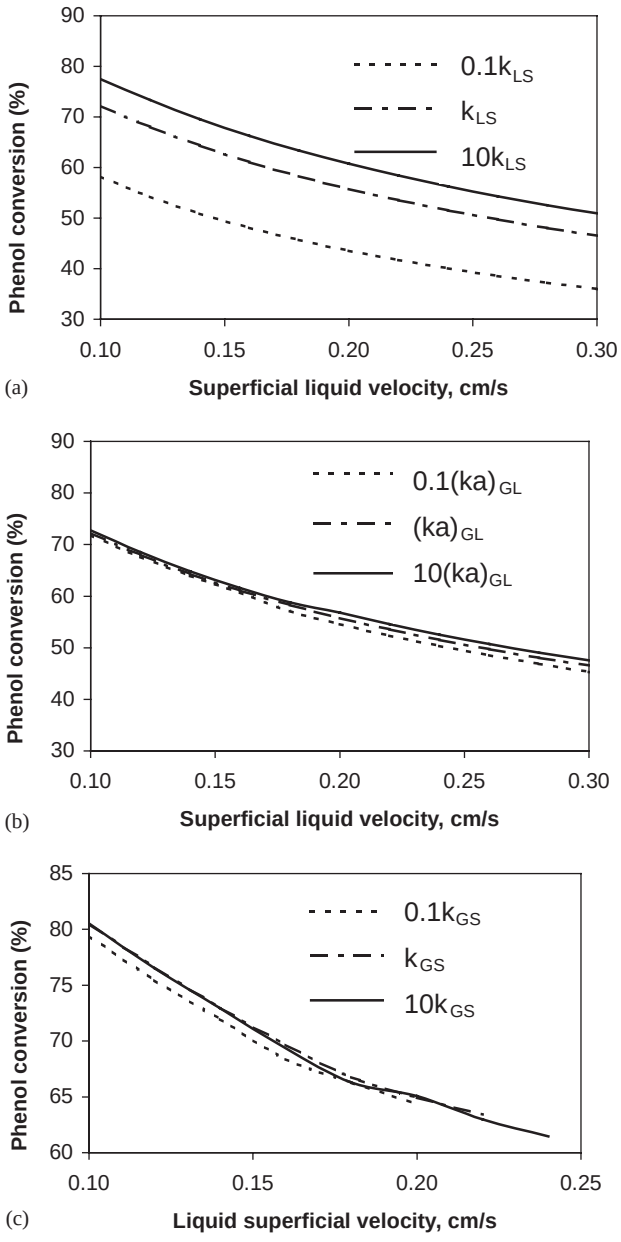

Fig. 18. Sensitivity of the models with regards to (a) liquid–solid, (b) gas–liquid, and (c) gas–solid mass transfer coefficients in trickle-bed reactor, $C_{B,0} = 6.0$ mol/m^3, time = 5 h, $P = 0.5$ MPa, $T = 80$°C.

4. Conclusion

In this work, a sequential approach has been developed for applying the ADM in combination with the pellet-scale model. The ADM predicted the local concentration along the reactor axis, whereas the pellet-scale model evaluated the local effectiveness factor corresponding to the local reactant concentration. Such a sequential approach incorporates the non-linear reaction kinetics expression into the pellet-scale model and the ADM, without any fitting parameter. Experimental observations for AMS hydrogenation have been used to validate the developed modeling scheme. The

comparable simulation results from the parallel and sequential approaches exhibit that both approaches are as good in terms of the simulation capability, and hence, they can be used for simulation for such reaction and others in packed-bed reactors. To account for unsteady-state reactor behavior, the sequential scheme was utilized to predict the catalytic wet oxidation of phenol in a packed-bed with newly developed but rapidly deactivated catalyst pellets of MnO_2/CeO_2. The simulation described the time evolution of catalyst deactivation at pellet scale along the reactor axis. The simulation suggests that liquid-reactant limited reactions such as wet oxidation can obtain higher conversion in a packed bubble column than in a trickle bed. However, a higher axial catalyst deactivation rate also results from the upflow mode than from the downflow mode. In both upflow and downflow, an increase of gas velocity does not affect the phenol conversion significantly, and the external mass transfer coefficients are dependent mostly on the liquid velocity. The MnO_2/CeO_2 catalyst is not applicable for the packed-bed operation, and its commercial application is unfeasible. A new catalyst is required for the CWO process. The proposed sequential approach will be used for the evaluation and design of the new catalyst, once the reaction kinetic expressions are available.

Notation

a	catalyst specific surface area per unit reactor bed, m^2/m^3
$c_{i,L}$	dimensionless concentration of species i in liquid
$C_{i,L}$	concentration of species i in liquid phase
d_p	particle diameter, m
D_{EL}	axial dispersion coefficient of the liquid phase, m^2/s
k, k'	lumped rate constant
$(ka)_{GL}$	gas–liquid mass transfer coefficient s^{-1}
k_{GS}	gas–solid mass transfer coefficient, m/s
k_{LS}	liquid–solid mass transfer coefficient, m/s
K, K'	adsorption equilibrium constants
L	reactor length, m
P	operating pressure, atm
Pe	Péclet number $\left(=\frac{u_{SL}L}{D_{EL}}\right)$
r_i	reaction rate based on the species i, $mol/m^3/s$ or mol/kg/min
t	reaction time, min
T	temperature, K
u_g	gas superficial velocity, m/s
u_{SL}	liquid superficial velocity, m/s
X	conversion of biphenyl, %
Z	bed axial position, m

Greek letters

$\alpha_{G,L}$	dimensionless parameter
$\alpha_{L,S}$	dimensionless parameter
β_1, β_2	dimensionless parameter
ε_B	bed porosity
εl	liquid holdup
η	reaction effectiveness factor
η_{CE}	catalyst wetting efficiency
φ	catalyst active site fraction
ξ	dimensionless position
v_B	stoichiometric coefficient for species B

Sub/superscripts

$*$	free site, adsorbed
A	gas reactant, H_2 or O_2
B	phenol
C	oxidation intermediate product
D	oxidation end-product lump
G	gas phase
L	liquid phase
S	solid phase
e	equilibrium
0	input

Acknowledgements

The financial supporters of the Chemical Reaction Engineering Lab (CREL) are gratefully acknowledged. Thanks are also given to Dr. Larachi for authorizing access to the source code for the parallel model scheme proposed in Iliuta and Larachi (2001).

References

Beaudry, E.G., Dudukovic, M.P., Mills, P.L., 1987. Trickle-bed reactors: liquid diffusional effects in a gas-limited reaction. A.I.Ch.E. Journal 33, 1435.

Bensetiti, Z., Larachi, F., Grandjean, B.P.A., Wild, G., 1997. Liquid saturation in cocurrent upflow fixed-bed reactors: a state-of-the-art correlation. Chemical Engineering Science 52, 4239.

Berger, R.J., Perez-Ramirez, J., Kapteijn, F., Moulijn, J.A., 2002. Catalyst performance testing: bed dilution revisited. Chemical Engineering Science 57, 4921.

Cassanello, M.C., Martinez, O.M., Cukierman, A.L., 1992. Effect of the liquid axial dispersion on the behavior of fixed bed three phase reactors. Chemical Engineering Science 47, 3331.

Dwivedi, P.N., Upadhyah, S.N., 1977. Particle-fluid mass transfer in fixed and fluidized beds. Industrial Engineering Chemistry Process Design and Development 16, 157.

El-Hisnawi, A.A., 1981. Tracer and reaction studies in trickle-bed reactors. D.Sc. Dissertation, Washington University, St. Louis, MS.

Froment, G.F., Depauw, G.A., Vanrysselberghe, V., 1994. Kinetic modeling and reactor simulation in hydrodesulfurization of oil fractions. Industrial and Engineering Chemistry Research 33, 2975.

Fukushima, S., Kusaka, K., 1977a. Liquid-phase volumetric and mass-transfer coefficient, and boundary of hydrodynamic flow region in packed column with cocurrent downward flow. Journal of Chemical Engineering of Japan 10, 468.

Fukushima, S., Kusaka, K., 1977b. Interfacial area and boundary of hydrodynamic flow region in packed column with cocurrent downward flow. Journal of Chemical Engineering of Japan 10, 461.

Goto, S., Smith, J.M., 1975. Trickle bed reactor performance Part II: reaction studies. A.I.Ch.E. Journal 21, 706.

Guo, J., Al-Dahhan, M., 2003. Catalytic wet oxidation of Phenol by hydrogen peroxide over pillared clay catalyst. Industrial and Engineering Chemistry Research 42, 2450–2460.

Hamoudi, S., Belkacemi, K., Larachi, F., 1999. Catalytic oxidation of aqueous phenolic solutions catalyst deactivation and kinetics. Chemical Engineering Science 54, 3569.

Hochman, J.M., Effron, E., 1969. Two-phase cocurrent downflow in packed-beds. Industrial and Engineering Chemistry Fundamentals 8, 63.

Iliuta, I., Larachi, F., 2001. Wet air oxidation solid catalysis analysis of fixed and sparged three-phase reactors. Chemical Engineering Processing 40, 175.

Iliuta, I., Thyrion, F.C., Muntean, O., 1996. Residence time distribution of the liquid in gas–liquid cocurrent upflow fixed-bed reactors. Chemical Engineering Science 51, 4579.

Khadilkar, M.R., Wu, Y.X., Al-Dahhan, M.H., Dudukovic, M.P., Colakyan, M., 1996. Comparison of trickle-bed and upflow reactor performance at high pressure: model predictions and experimental observation. Chemical Engineering Science 51, 2139.

Larachi, F., Iliuta, I., Belkacemi, K., 2001. Catalytic wet air oxidation with a deactivating catalyst analysis of fixed and sparged three-phase reactors. Catalysis Today 64, 309.

Lemcoff, N.O., Cukierman, A.L., Martinez, O.M., 1988. Effectiveness factor of partially wetted catalyst particles: evaluation and application to the modeling of trickle bed reactors. Catalysis Reviews: Science and Engineering 30, 393.

Levec, J., Smith, J.M., 1976. Oxidation of acetic acid solutions in a trickle-bed reactor. A.I.Ch.E. Journal 22, 159.

Maugans, C.B., Akgerman, A., 2003. Catalytic wet oxidation of phenol in a trickle bed reactor over a Pt/TiO_2 Catalyst. Water Research 37, 319.

Mears, D.E., 1971. Tests for transport limitations in experimental catalytic reactors. Industrial engineering chemistry process design and development 10, 541.

Pintar, A., Levec, J., 1992. Catalytic oxidation of organics in aqueous solutions: kinetics of phenol oxidation. Journal of Catalysts 135, 345.

Pintar, A., Levec, J., 1994. Catalytic liquid-phase oxidation of phenol aqueous solutions: a kinetic investigation. Industrial and Engineering Chemistry Research 33, 3070.

Pintar, A., Bercic, G., Levec, J., 1997. Catalytic liquid-phase oxidation of aqueous phenol solutions in a trickle-bed. Chemical Engineering Science 52, 4143.

Rajashekharam, M.V., Jaganathan, R., Chaudhari, R.V., 1998. A trickle-bed reactor model for hydrogenation of 2,4 dinitrotoluene: experimental verification. Chemical Engineering Science 53, 787.

Ramachandran, P.A., Chaudhari, R.V., 1983. Three-phase Catalytic Reactors. Gordon and Breach Science Publishers, New York.

Ramachandran, P.A., Smith, J.M., 1979. Effectiveness factors in trickle bed reactors. A.I.Ch.E. Journal 25, 538.

Reid, R.C., Prausnitz, J.M., Poliing, B.E., 1986. The Properties of Gases and Liquids, 4th Edition. McGraw-Hill, New York, USA.

Reiss, L.P., 1967. Concurrent gas-liquid contacting in packed columns. Industrial Engineering Chemistry Process Design and Development 6, 486.

Specchia, V., Baldi, G., Glanetto, A., 1978. Solid-liquid mass transfer in concurrent two-phase flow through packed beds. Industrial Engineering Chemistry Process Design and Development 17, 362.

Stuber, F., Wilhelm, A.M., Delmas, H., 1996. Modeling of three phase catalytic upflow reactor: a significant chemical determination of liquid–solid and gas–liquid mass transfer coefficients. Chemical Engineering Science 51, 2161.

Tan, C.S., Smith, J.M., 1980. Catalyst particle effectiveness with unsymmetrical boundary conditions. Chemical Engineering Science 35, 1601.

Toppinen, S., Aittamaa, J., Salmi, T., 1996. Interfacial mass transfer in trickle-bed reactor modeling. Chemical Engineering Science 51, 4335.

Villadsen, J., Michelsen, M.L., 1978. Solution of Differential Equation Models by Polynomial Approximation. Prentice-Hall, NJ, USA.

Yurii, I.M.M., Moshe, S., 1998. Catalytic abatement of water pollutants. Industrial and Engineering Chemistry Research 37, 309.